Article

# The Hydrogen-Bonding Network in Heme Oxygenase Also Functions as a Modulator of Enzyme Dynamics: Chaotic Motions upon Disrupting the H-Bond Network in Heme Oxygenase from *Pseudomonas aeruginosa*

, Yuhong Zeng, Angela Wilks, and Mario Rivera

*J. Am. Chem. Soc.*, **2007**, 129 (38), 11730-11742• DOI: 10.1021/ja072405q • Publication Date (Web): 01 September 2007



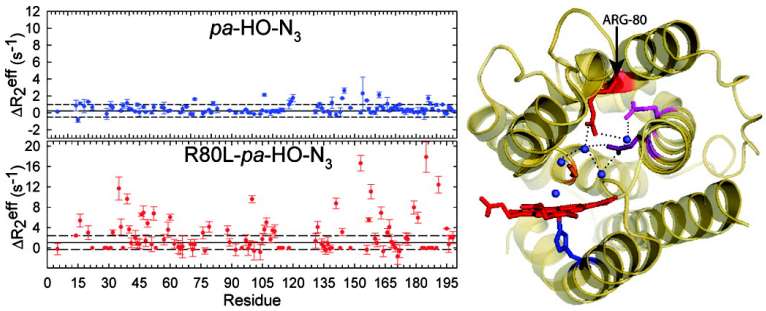


## More About This Article

Additional resources and features associated with this article are available within the HTML version:

- Supporting Information
- Links to the 3 articles that cite this article, as of the time of this article download
- Access to high resolution figures
- Links to articles and content related to this article
- Copyright permission to reproduce figures and/or text from this article

View the Full Text HTML

J|A|C|S
ARTICLES
Published on Web 09/01/2007

# The Hydrogen-Bonding Network in Heme Oxygenase Also Functions as a Modulator of Enzyme Dynamics: Chaotic Motions upon Disrupting the H-Bond Network in Heme Oxygenase from *Pseudomonas aeruginosa*

Juan Carlos Rodríguez,[†] Yuhong Zeng,[†] Angela Wilks,[‡] and Mario Rivera*,[†]

*Contribution from the Ralph N. Adams Institute for Bioanalytical Chemistry and Department of Chemistry, University of Kansas, Multidisciplinary Research Building, 2030 Becker Drive, Room 220 E, Lawrence, Kansas 66047, and Department of Pharmaceutical Sciences, School of Pharmacy, University of Maryland, Baltimore, Maryland 21201-1180*

Received April 5, 2007; E-mail: mrivera@ku.edu

***Abstract:*** Relaxation compensated Carr−Purcell−Meiboom−Gill (rc-CPMG) NMR experiments have been used to investigate $\mu$s−ms motions in heme oxygenase from *Pseudomonas aeruginosa* (*pa*-HO) in its ferric state, inhibited by $CN^-$ (*pa*-HO−CN) and $N_3^-$ (*pa*-HO−$N_3$), and in its ferrous state, inhibited by CO (*pa*-HO−CO). Comparative analysis of the data from the three forms indicates that the nature of the coordinated distal ligand affects the $\mu$s−ms conformational freedom of the polypeptide in regions of the enzyme far removed from the heme iron and distal ligand. Interpretation of the dynamical information in the context of the crystal structure of resting state *pa*-HO shows that residues involved in the network of structural hydrogen-bonded waters characteristic of HOs undergo $\mu$s−ms motions in *pa*-HO−CN, which was studied as a model of the highly paramagnetic $S = {}^5/_2$ resting state form. In comparison, similar motions are suppressed in the *pa*-HO−CO and *pa*-HO−$N_3$ complexes, which were studied as mimics of the obligatory oxyferrous and ferric hydroperoxide intermediates, respectively, in the catalytic cycle of heme degradation. These findings suggest that in addition to proton delivery to the nascent $Fe^{III}$−$OO^-$ intermediate during catalysis, the hydrogen-bonding network serves two additional roles: (*i*) propagate the electronic state (reactive state) in each of the distinct steps of the catalytic cycle to key but remote sections of the polypeptide via small rearrangements in the network of hydrogen bonds and (*ii*) modulate the conformational freedom of the enzyme, thus allowing it to adapt to the demanding changes in axial coordination state and substrate transformations that take place during the catalytic cycle. This idea was probed by disrupting the hydrogen-bonding network in *pa*-HO by replacing R80 with L. NMR spectroscopic studies conducted with R80L-*pa*-HO−$N_3$ and R80L-*pa*-HO−CO revealed that the mutant exhibits nearly global conformational disorder, which is absent in the equivalent complexes of the wild type enzyme. The "chaotic" disorder in the R80L mutant is likely related to its significantly lower efficiency to hydroxylate heme in the presence of $H_2O_2$, relative to the wild type enzyme.

Heme oxygenase is a ubiquitous enzyme in mammals, plants, insects, fungi, and bacteria, which functions by capturing heme for subsequent degradation of the macrocycle and release of the iron. Two isoforms are known in mammals, HO-1 and HO-2.[1] The former is the most actively investigated because it is induced by numerous stimuli such as heme, metals, hormones, and oxidizing agents.[2] HO-2 is constitutively expressed and is present in highest concentration in testes and the brain.[2] In mammals HO activity is crucial for the recycling of iron because approximately 3% of the daily iron requirement is obtained from dietary intakes.[3] The other products of heme degradation are also important physiologically; biliverdin and its redox couple, bilirubin, are powerful antioxidants,[4,5] and carbon monoxide (CO) is thought to play important roles as a neural messenger[6] and has been implicated as a protective agent in hemorrhagic shock[7] and as a modulator of vascular tone.[8,9]

Heme oxygenase has also been identified in some pathogenic bacteria, where it aids in overcoming a primary obstacle for successful colonization of a mammalian host (infection), namely, the lack of available free iron, which in mammals is maintained at a very low level, $\sim 10^{-9}$ M.[10] Many pathogenic bacteria

[†] University of Kansas.
[‡] University of Maryland.

(1) Maines, M. D. *Annu. Rev. Pharmacol. Toxicol.* **1997**, *37*, 517−554.
(2) Otterbein, L. E.; Choi, A. M. K. *Am. J. Physiol. Lung Cell Mol. Physiol.* **2000**, *279*, L1029−L1037.
(3) Uzel, C.; Conrad, M. E. *Semin. Hematol.* **1998**, *35*, 27−34.
(4) Stocker, R.; Yamamoto, Y.; McDonagh, A. F.; Glazer, A. N.; Ames, B. N. *Science* **1987**, *235*, 1043−1046.
(5) Marilena, G. *Biochem. Mol. Med.* **1997**, *61*, 136−142.
(6) Verma, A.; Hirsch, D. J.; Glatt, C. E.; Ronnett, G. V.; Snyder, S. H. *Science* **1993**, *259*, 381−384.
(7) Pannen, B. H. J.; Köhler, N.; Hole, B.; Bauer, M.; Clemens, M. G.; Geiger, K. K. *J. Clin. Invest.* **1998**, *102*, 1220−1228.
(8) Kaide, J.-I.; Zhang, F.; Wei, Y.; Jiang, H.; Yu, C.; Wang, W.; Balazy, M.; Abraham, N. G.; Nasjletti, A. *J. Clin. Invest.* **2001**, *107*, 1163−1171.
(9) Zhang, F.; Kaide, J.-I.; Rodriguez-Mulero, F.; Abraham, N. G.; Nasjletti, A. *Am. J. Hypertens.* **2001**, *14*, 62S−67S.


**10.1021/ja072405q CCC: $37.00** 

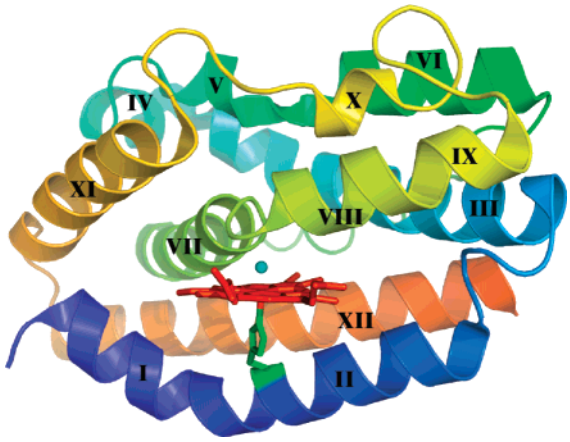


***Figure 1.*** Structure of *pa*-HO in its ferric resting state (PDB:1SK7) illustrating the α-helical fold, the positioning of the heme, and the axial coordination by a His-imidazole and water ligands. The heme is "sandwiched" between the proximal helices (I and II) and the distal helices (VII and VIII). The loop between the two distal helices is typically referred to as the helix kink.

possess specific heme uptake systems to mine heme-iron for their metabolic needs. These systems are perhaps best understood in gram negative bacteria,[11] which express highly specific outer membrane receptors that bind different heme-proteins, extract their heme, and transport it into the bacterial periplasm.[12−14] In agreement with this view, a report indicates that heme iron is the preferred iron source during the initiation of infection by *Staphylococcus aureus*.[15] Nevertheless, a relatively small number of bacterial HOs have been identified thus far.[14,16−19] In addition, heme oxygenase seems to be present ubiquitously in the plant kingdom,[20,21] where its main role may be the degradation of heme to biliverdin, which is subsequently used in the synthesis of phycobilins and open-chain tetrapyrroles.[22]

The structures of heme oxygenase enzymes, from mammals and from bacteria, are very similar. HO harbors the heme in a highly α-helical fold between the proximal and distal helices, I and II, and VII and VIII, respectively (Figure 1). The proximal helix harbors a non-ionized His ligand that coordinates the heme iron. In the resting state, the ferric ion is coordinated by a $H_2O$ distal ligand; however it is important to appreciate that the nature of this ligand changes several times during the catalytic cycle of heme degradation (see below). HO is devoid of a distal residue which in other heme enzymes and proteins plays an important role in stabilizing the distal ligand. Thus, in HO the role of stabilizing the distal ligand appears to rest mainly in a conserved Gly residue ($Gly^{143}$ in mammalian HOs,[23,24] $Gly^{125}$ in HO from *P. aeruginosa*[25,26]) and in a network of hydrogen-bonded structural waters that extends from the distal ligand to the surface of the enzyme. The presence of structural waters networked by hydrogen bonds in the distal site has been observed in all HOs with known structure, both in the crystal structures[26−29] and in solution.[30−32] However, in agreement with the very low sequence similarity among HOs from different organisms[33] the nature of residues participating in the hydrogen bond network is not conserved among the different structures. This indicates that although conservation of the network is very important to HO function, the details of how this is achieved in each enzyme are rather flexible. Nevertheless, disruption of the hydrogen-bonding network results in significant or total loss of HO activity, as has been observed upon mutation of Asp-140 in mammalian HOs for residues with side chains not capable of participating in hydrogen bonding.[34,35] Along the same vein, it has been suggested that in the structure of HO from *Neisseriae meningitidis* (*nm*-HO) Arg-77 may play a role similar that of Asp-140 in mammalian HOs. The side chain of Arg-77 in *nm*-HO relocates when the oxidation state or axial ligand coordination state of the enzyme is altered, with concomitant rearrangement of the details in the hydrogen-bonding network.[36] Inspection of the *Pseudomonas aeruginosa* HO (*pa*-HO) reveals that the residue equivalent to Arg-77 in *nm*-HO, Arg-80, is also intimately involved in stabilizing the network of structural waters in this enzyme. Indeed, it will be shown below that replacement of Arg-80 for Leu brings a significant decrease in the ability of the enzyme to catalyze heme hydroxylation, thus implicating this residue as an important component of the hydrogen-bonding network in *pa*-HO.

The initial steps of dioxygen activation that lead to heme breakdown by HO are similar those followed by monooxygenases (i.e., cytochrome P450) (Figure 2): The ferric (resting state) enzyme is reduced to its ferrous form, with concomitant loss of the distal ligand to produce a pentacoordinated ferrous heme−HO complex. Molecular oxygen ($O_2$) binds to the ferrous iron to form an oxyferrous ($Fe^{II}—O_2$) complex, which accepts an electron, rearranges its electronic structure, and accepts a proton to form a highly reactive ferric hydroperoxide ($Fe^{III}$—OOH) complex.[37] At this stage in the reaction the mechanisms of heme oxygenation and monooxygenation diverge: Whereas

(10) Chipperfield, J. R.; Ratledge, C. *BioMetals* **2000**, *13*, 165−168.
(11) Schryvers, A. B.; Stojiljkovic, I. *Mol. Microbiol.* **1999**, *32*, 1117−1123.
(12) Lee, C. L. *Mol. Microbiol.* **1995**, *18*, 383−390.
(13) Stojiljkovic, I.; Hantke, K. *EMBO J.* **1992**, *11*, 4359−4367.
(14) Zhu, W.; Hunt, D. J.; Richardson, A. R.; Stojiljkovic, I. *J. Bacteriol.* **2000**, *182*, 439−447.
(15) Skaar, E. P.; Humayun, M.; Bae, T.; DeBord, K. L.; Schneewind, O. *Science* **2004**, *305*, 1626−1628.
(16) Schmitt, M. P. *J. Bacteriol.* **1997**, *179*, 838−845.
(17) Ratliff, M.; Zhu, W.; Deshmukh, R.; Wilks, A.; Stojiljkovic, I. *J. Bacteriol.* **2001**, *183*, 6394−6403.
(18) Skaar, E. P.; Gaspar, A. H.; Schneewind, O. *J. Biol. Chem.* **2004**, *279*, 436−443.
(19) Suits, M. D.; Pal, G. P.; Nakatsu, K.; Matte, A.; Cygler, M.; Jia, Z. *Proc. Natl. Acad. Sci. U.S.A.* **2005**, *102*, 16955−16960.
(20) Cornejo, J.; Beale, S. I. *Photosynth. Res.* **1997**, *51*, 223−230.
(21) Muramoto, T.; Kohchi, T.; Yokota, A.; Hwang, I.; Goodman, H. M. *Plant Cell* **1999**, *11*, 335−347.
(22) Beale, S. I. *Chem. Rev.* **1993**, *93*, 785−802.
(23) Schuller, D. J.; Wilks, A.; Ortiz de Montellano, P. R.; Poulos, T. L. *Nat. Struct. Biol.* **1999**, *6*, 860−867.
(24) Sugishima, M.; Sakamoto, H.; Higashimoto, Y.; Omata, Y.; Hayashi, S.; Noguchi, M.; Fukuyama, K. *J. Biol. Chem.* **2002**, *277*, 45086−45090.
(25) Rodriguez, J. C.; Wilks, A.; Rivera, M. *Biochemistry* **2006**, *45*, 4578−4592.
(26) Friedman, J.; Lad, L.; Li, H.; Wilks, A.; Poulos, T. L. *Biochemistry* **2004**, *43*, 5239−5245.
(27) Schuller, D. J.; Zhu, W.; Stojiljkovic, I.; Wilks, A.; Poulos, T. L. *Biochemistry* **2001**, *40*, 11552−11558.
(28) Sugishima, M.; Omata, Y.; Kakuta, Y.; Sakamoto, H.; Noguchi, M.; Fukuyama, K. *FEBS Lett.* **2000**, *471*, 61−66.
(29) Hirotsu, S.; Chu, G. C.; Unno, M.; lee, D.-S.; Yoshida, T.; Park, S.-Y.; Shiro, Y.; Ikeda-Saito, M. *J. Biol. Chem.* **2004**, *279*, 11937−11947.
(30) Syvitski, R. T.; Li, Y.; Auclair, K.; Ortiz de Montellano, P. R.; La Mar, G. N. *J. Am. Chem. Soc.* **2002**, *124*, 14296−14297.
(31) Li, Y.; Syvitski, R. T.; Chu, G. C.; Ikeda-Saito, M.; La Mar, G. N. *J. Biol. Chem.* **2003**, *278*, 6651−6663.
(32) Li, Y.; Syvitski, R. T.; Auclair, K.; Wilks, A.; Ortiz de Montellano, P. R.; La Mar, G. N. *J. Biol. Chem.* **2002**, *277*, 33018−33031.
(33) Rivera, M.; Zeng, Y. *J. Inorg. Biochem.* **2005**, *99*, 337−354.
(34) Koenigs Lightning, L.; Huang, H.; Moënne-Loccoz, P.; Loehr, T. M.; Schuller, D. J.; Poulos, T. L.; Ortiz de Montellano, P. R. *J. Biol. Chem.* **2001**, *276*, 10612−10619.
(35) Fujii, H.; Zhang, X.; Tomita, T.; Ikeda-Saito, M.; Yoshida, T. *J. Am. Chem. Soc.* **2001**, *123*, 6475−6484.
(36) Friedman, J.; Lad, L.; Deshmukh, R.; Li, H.; Wilks, A.; Poulos, T. L. *J. Biol. Chem.* **2003**, *278*, 34654−34659.
(37) Yoshida, T.; Noguchi, M.; Kikuchi, G. *J. Biol. Chem.* **1980**, *255*, 4418−4420.

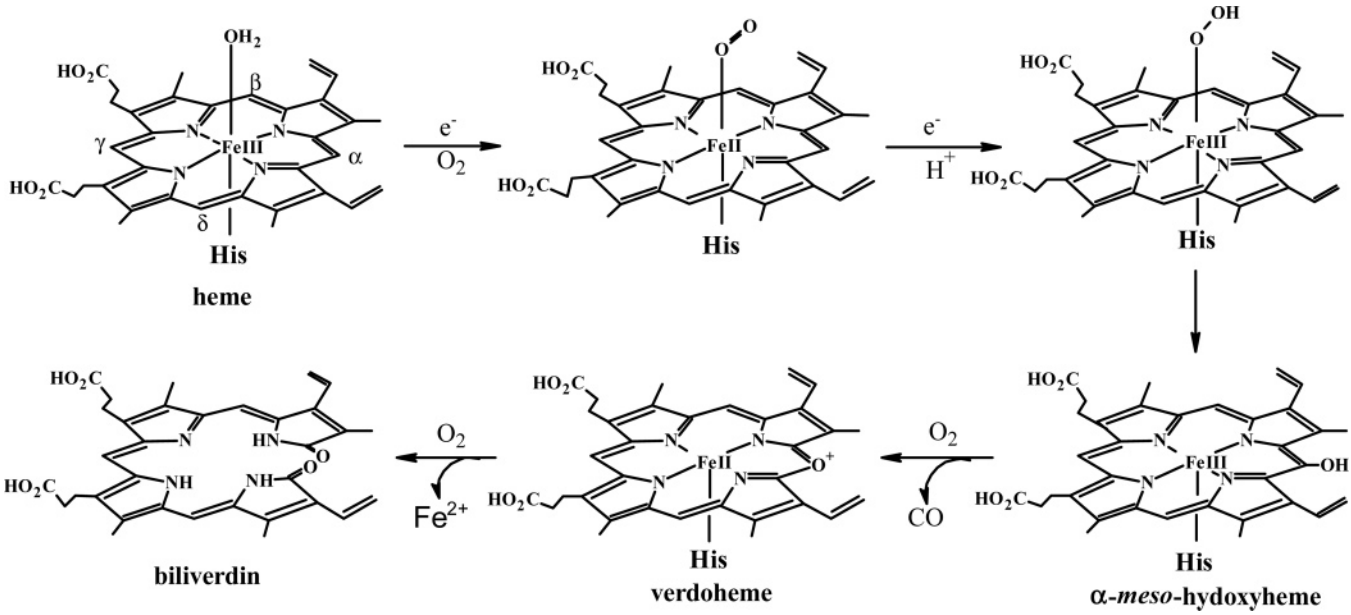


***Figure 2.*** Heme degradation path, as catalyzed by HO. The proximal coordination (His) is maintained during the entire cycle, whereas the nature of the distal ligand changes several times. The substrate (heme) also undergoes several structural changes during the catalytic cycle, including meso carbon hydroxylation, ring contraction upon formation of verdoheme, and, finally, ring opening and loss of iron to form biliverdin.

the $Fe^{III}$—OOH oxidizing species in monooxygenases decays to an oxoferryl species ($Fe^{V}$=O), the $Fe^{III}$—OOH intermediate in HO reacts with heme to produce meso-hydroxyheme. The latter undergoes a subsequent $O_2$-dependent elimination of the hydroxylated meso carbon as CO, with concomitant formation of hexacoordinated verdoheme[38] (Figure 2). Verdoheme is subsequently oxidized to $Fe^{III}$—biliverdin in a reaction that requires both $O_2$ and reducing equivalents.[37,39] In this context, it is interesting that a surrogate reaction between HO ($Fe^{III}$ resting state) and $H_2O_2$ has been shown to promote meso hydroxylation of heme;[40] addition of 1 equiv of $H_2O_2$ to HO-1 under anaerobic conditions hydroxylates the macrocycle to meso-hydroxyheme, via the formation of an $Fe^{III}$—OOH intermediate. Subsequent introduction of air to the sample promotes the rapid conversion of meso-hydroxyheme to verdoheme. This surrogate reaction has also been observed with all bacterial HOs and has been used for the efficient preparation of verdoheme.[38,41]

A very interesting feature of the complicated catalytic cycle of HO is the fact that the enzyme acts on a large substrate (heme) and has to adapt to several changes in substrate structure that range from axial ligand replacements, i.e., $H_2O$ in the resting state, $O_2$ in the ferrous state, $OO^{2-}$ and $HOO^-$ in the ferric activated complex, to several changes in the macrocycle, which include heme hydroxylation, ring contraction (verdoheme), and ring opening (biliverdin). A series of NMR spectroscopic studies have been undertaken with the aim of understanding how changes in axial coordination affect heme electronic structure and therefore reactivity in HO.[25,33,42,43] The large number of unpaired electrons ($S = {}^5/_2$) in the resting state form of the enzyme cause many resonances in relative close proximity to the heme to become undetectable.[44] Consequently, the resting state is typically studied by NMR spectroscopy using the cyanide-inhibited form of the enzyme ($S = {}^1/_2$).[45−48] The oxyferrous form is susceptible to autoxidation processes that produce resting state enzyme and superoxide; hence, this form of the enzyme is typically studied using the ferrous carbomonoxy complex ($Fe^{II}$—CO).[36,49] The hydroxide ($Fe^{III}$—OH) and azide ($Fe^{III}$—$N_3$) complexes of *Pseudomonas aeruginosa*-HO, *pa*-HO—OH, and *pa*-HO—$N_3$, respectively, have been used to approximate the heme electronic properties of the highly reactive $Fe^{III}$—OOH oxidizing species.[42,43] Results from these studies showed that axial ligands capable of accepting a hydrogen bond at the coordinating atom, such as $OH^-$ or $N_3^-$, have a profound influence in the electronic structure of the heme. Thus, it was suggested that if the $HOO^-$ ligand brings about similar electronic structures the unpaired spin density at the meso carbons would facilitate homolytic cleavage of the O—O bond by efficiently trapping the •OH radical at a sterically unprotected meso carbon.[33,42,43,50] This notion put forward from experimental studies is in good agreement with theoretical studies suggesting that heme hydroxylation by HO is more likely to occur via a stepwise mechanism in which homolytic cleavage of the O—O bond is followed by trapping the •OH radical at the porphyrin.[51]

(38) Damaso, C. O.; Bunce, R. A.; Barybin, M. V.; Wilks, A.; Rivera, M. *J. Am. Chem. Soc.* **2005**, *127*, 17852−17853.
(39) Yoshida, T.; Kikuchi, G. *J. Biol. Chem.* **1978**, *253*, 4230−4236.
(40) Wilks, A.; Ortiz de Montellano, P. R. *J. Biol. Chem.* **1993**, *268*, 22357−22362.
(41) Damaso, C. O.; Rubie, N. D.; Moënne-Loccoz, P.; Rivera, M. *Inorg. Chem.* **2004**, *43*, 8470−8478.
(42) Caignan, G. A.; Deshmukh, R.; Zeng, Y.; Wilks, A.; Bunce, R. A.; Rivera, M. *J. Am. Chem. Soc.* **2003**, *125*, 11842−11852.
(43) Zeng, Y.; Caignan, G. A.; Bunce, R. A.; Rodriguez, J. C.; Wilks, A.; Rivera, M. *J. Am. Chem. Soc.* **2005**, *127*, 9794−9807.
(44) Liu, Y.; Zhang, X.; Yoshida, T.; La Mar, G. N. *J. Am. Chem. Soc.* **2005**, *127*, 6409−6422.
(45) Caignan, G. A.; Deshmukh, R.; Wilks, A.; Zeng, Y.; Huang, H.; Moënne-Loccoz, P.; Bunce, R. A.; Eastman, M. A.; Rivera, M. *J. Am. Chem. Soc.* **2002**, *124*, 14879−14892.
(46) Zeng, Y.; Deshmukh, R.; Caignan, G. A.; Bunce, R. A.; Rivera, M.; Wilks, A. *Biochemistry* **2004**, *43*, 5222−5238.
(47) Li, Y.; Syvitski, R. T.; Auclair, K.; Ortiz de Montellano, P. R.; La Mar, G. N. *J. Am. Chem. Soc.* **2003**, *125*, 13392−13403.
(48) Gorst, C. M.; Wilks, A.; Yeh, D. C.; Ortiz de Montellano, P. R.; La Mar, G. N. *J. Am. Chem. Soc.* **1998**, *120*, 8875−8884.
(49) Sugishima, M.; Sakamoto, H.; Noguchi, M.; Fukuyama, K. *Biochemistry* **2003**, *42*, 9898−9905.
(50) Rivera, M.; Caignan, G. A.; Astashkin, A. V.; Raitsimring, A. M.; Shokhireva, T. K.; Walker, F. A. *J. Am. Chem. Soc.* **2002**, *124*, 6077−6089.
(51) Sharma, P. K.; Kevorkiants, R.; de Visser, S. P.; Kumar, D.; Shaik, S. *Angew. Chem., Int. Ed.* **2004**, *43*, 1129−1132.

Moreover, additional calculations[52] suggest that homolytic cleavage of the O−O bond proceeds via a species with an electronic structure resembling a porphyrin radical, $Por^{+\bullet}Fe^{III}$-OH—HO•. This convergence of ideas from independent experimental and theoretical studies suggests *pa*-HO−OH and *pa*-HO−$N_3$ as reasonable models of the highly reactive $Fe^{III}$−OOH intermediate.

The above-described NMR studies, which were centered mainly on observing the heme active site in *pa*-HO, were followed by a study aimed at probing the polypeptide in *pa*-HO−CN and *pa*-HO−$N_3$. Global probing of the polypeptide in these complexes by hydrogen−deuterium (H/D) exchange experiments led to the surprising observation that the *pa*-HO−$N_3$ complex is significantly more protected toward H/D exchange than its *pa*-HO−CN counterpart.[25] Several of the residues exhibiting higher protection factors in *pa*-HO−$N_3$ relative to *pa*-HO−CN are far from the heme, suggesting that the nature of the distal ligand, the diatomic $CN^-$ or the triatomic $N_3^-$, influence polypeptide dynamics distinctly. Moreover, residues far away from the heme that exhibit higher protection factors in *pa*-HO−$N_3$ relative to *pa*-HO−CN appear to be in "communication" with the distal ligand via structural waters that form part of the hydrogen-bonding network. This network which is characteristic of HO enzymes is thought to function in the delivery of a $H^+$ to the nascent $Fe^{III}$−$OO^-$, in order to form the $Fe^{III}$−OOH oxidizing species. The surprising findings revealed by H/D exchange experiments led to the suggestion that proton delivery is not the only function of the network of structural waters in HO. Instead, it was proposed that an additional function of the structural waters is to provide adaptable interactions between otherwise remote structural elements, thus permitting rapid propagation of conformational changes in the active site to remote but key structural elements in the enzyme, with minimum perturbation of the secondary structure.[25]

Consequently, the studies described herein were conducted with the aim of probing whether perturbations in the hydrogen-bonding network bring changes in the equilibrium conformational dynamics of *pa*-HO that are manifested in an altered reactivity. Results from these studies show that the nature of the distal ligand indeed exerts an effect in the conformational flexibility of the *pa*-HO polypeptide in regions of the enzyme that although far removed form the heme center, remain "in communication" via the network of hydrogen-bonded waters. In addition, these investigations revealed that disruption of the hydrogen-bonding network in *pa*-HO brought about by replacing Arg-80 for Leu triggers pronounced conformational disorder in the enzyme, which is likely related to the low efficiency of heme hydroxylation observed with the Arg80Leu mutant of *pa*-HO.

## Experimental Methods

**Site Directed Mutagenesis.** The R80L mutant of *pa*-HO was prepared using the QuikChange mutagenesis kit (Stratagene; La Jolla, CA) and DNA primers GGCTTCCCGCGCCCTGGACGAC-GCCGC-CG-3′ (sense) and 5′-CGAGCGGCGTCGTCCAGGGCGCGGGAAGCC-3′ (anti-sense).

**Sample Preparation.** Isotopically enriched *pa*-HO and R80L-*pa*-HO were expressed in *E. coli* BL21(DE3) gold and purified by ion exchange and size exclusion chromatography as described previously.[25] The R80L-*pa*-HO−heme complex was subjected to a second purification step. Briefly, the R80L-*pa*-HO−heme complex was loaded on a column packed with ion-exchange resin (DE-52) previously equilibrated with 20 mM Tris, pH 7.4 (buffer A). The column was then equilibrated with buffer A containing 8 M urea. The unfolded protein, devoid of heme, was eluted from the ion-exchange resin with buffer A containing 0.3 M NaCl. The chromatographic fractions with $A_{280\ nm} > 0$ were pooled and dialyzed two times against 4 L of water to refold the protein and one final time against 4 L of 50 mM sodium phosphate, pH 7.0. The refolded protein was then reconstituted with heme and purified by size exclusion chromatography using a Sephacryl S-100 column equilibrated with 50 mM sodium phosphate, pH 7.0. The "unfold−refold" treatment described here afforded samples of R80L-*pa*-HO that typically produced better quality HSQC spectra than those prepared following the previously reported[45] purification procedure for wild type *pa*-HO.

**Preparation of the Ferrous *pa*-HO−CO Complex.** Samples of ferrous *pa*-HO−CO were prepared under anaerobic conditions inside a glovebox (Coy). All solutions and materials employed in the preparation of the complex were left inside a glovebox under anaerobic conditions overnight, while the protein solution (450 $\mu$L of 2 mM resting state *pa*-HO, dissolved in 50 mM phosphate buffer, pH 7.0) was placed inside 8 h prior to the start of the procedure. The solution containing resting state enzyme was bubbled with approximately 2 mL of CO, followed by addition of dithionite (∼2 mg in powder form) to reduce the heme iron to the ferrous ($Fe^{II}$) state, and subsequently bubbled with an additional 2 mL of CO. A 5 mL plastic syringe equipped with a metallic needle was used to draw CO from a round-bottom flask, which had been filled with CO outside the glovebox, capped with a rubber septum, and transferred inside the glovebox prior to the start of the procedure. Excess dithionite was eliminated by loading the resultant solution into a 2 mL spin column (Pierce; Rockford, IL) equilibrated with 8 mL of 50 mM phosphate buffer (pH 7.0) previously saturated with CO by bubbling, followed by eluting the ferrous *pa*-HO−CO complex with 2 mL of CO-saturated phosphate buffer. The first drop with a light pink color was discarded, and the following 500 $\mu$L were collected. This solution was bubbled again with CO, combined with 40 $\mu$L of $D_2O$, bubbled with CO, and transferred to a screw-capped NMR tube (Wilmad Lab Glass; Buena, NJ). The airtight seal in the NMR tube was reinforced by wrapping Teflon tape and Parafilm around the screw cap. Solutions of ferrous *pa*-HO−CO prepared in this fashion were stable for at least 3 weeks or longer when stored at 4 °C. The integrity of the sample was assessed from the appearance of the $^1H$−$^{15}N$ HSQC spectrum. Features in the HSQC spectrum attributable to paramagnetic species, which are well-known from work performed with the ferric state (unpublished results), were not present in spectra from samples collected 1 month after sample preparation.

**NMR Spectroscopy.** NMR experiments utilized for assigning the backbone resonances in ferrous *pa*-HO−CO were carried out at a 600 MHz $^1H$ frequency on a Varian Inova 600 spectrometer equipped with a triple resonance probe. Triple resonance experiments used to carry out the assignments were: HNCA, HN(CO)CA, HNCACB, and CBCA-(CO)NH. Relaxation compensated Carr−Purcell−Meiboom−Gill (CPMG) experiments were collected at a 600 MHz $^1H$ frequency on a Varian Unity Inova spectrometer equipped with a triple resonance probe. Duplicate experiments were collected at $\nu_{CPMG}$ fields of 25 and 600 Hz employing the TROSY version of a constant-time pulse sequence,[53] as implemented in the Varian Biopack software package. The constant time period was 80 ms, the relaxation delay, 2.2 s and the acquisition time, 120 ms, acquired over spectral widths of 10.8 ($^1H$) and 2.2 ($^{15}N$) kHz. Spectra were collected in interleave mode, alternating low and high $\nu_{CPMG}$ fields (i.e., 25 Hz, 600 Hz, 25 Hz, 600 Hz, etc). The refocusing $^{15}N$ $\pi$ pulse centered at each $\tau_{cp}$-180-$\tau_{cp}$ CPMG element

(52) Kumar, D.; de Visser, S. P.; Shaik, S. *J. Am. Chem. Soc.* **2005**, *127*, 8204−8213.

(53) Tollinger, M.; Skrynnikov, N. R.; Mulder, F. A. A.; Forman-Kay, J. D.; Kay, L. E. *J. Am. Chem. Soc.* **2001**, *123*, 11341−11352.

was applied with a field strength of 4.39 kHz. A total of 16 scans (preceded by 128 dummy scans) were collected for each of the 128 $t_1$ increments, resulting in a duration of approximately 3 h per experiment.

Exchange of longitudinal $^{15}$N magnetization between interconverting conformers at equilibrium was assessed with the aid of a two-dimensional $^1$H−$^{15}$N correlation $N_z$ exchange experiment.[54,55] The experiment was carried out at an 800 MHz $^1$H frequency on a Bruker Avance 800 spectrometer equipped with a cryoprobe. A pulse sequence that includes a semiconstant time frequency labeling period was used in order to achieve improved resolution along the $^{15}$N dimension.[56] Spectra were collected as matrices of 256 × 2496 complex points over spectral widths of 3.2 ($^{15}$N) and 12.8 ($^1$H) kHz with 16 scans per increment. The mixing time was 230 ms, and the relaxation delay, 1.2 s. All NMR spectra were processed using NMRPipe software applying mirror image linear prediction to double the number of t1 points. Further details appear in the corresponding figure captions. All experiments were performed at 32 °C with samples containing 1.3−1.8 mM protein, 50 mM sodium phosphate, pH 7.0, and 5−10% $D_2O$.

**Relaxation Data Analysis.** Spectra were processed using NMRPipe and analyzed using Sparky. Spectra were processed with a 90° shifted sine bell squared window function in each dimension and zero-filled to twice the number of points. The intensity of well-resolved cross-peaks was obtained directly from a table created by utilizing the peak picking and centering feature implemented in Sparky. Peak intensities obtained from spectra collected at each effective field were used to compute $\Delta R_2^{\text{eff}}(\nu_{\text{CPMG}})$ values from eq 1,[57−59] where $I_{25}$ and $I_{600}$ are the intensities of cross-peaks in spectra collected at effective CPMG fields of 25 and 600 Hz, respectively, and $T_{\text{cp}}$ is the constant time period in the experiments (80 ms).

$$\Delta R_2^{\text{eff}}(\nu_{\text{CPMG}}) = \frac{1}{T_{\text{cp}}} \ln\left(\frac{I_{600}}{I_{25}}\right) \quad (1)$$

## Results

**Backbone Resonance Assignments of *pa*-HO−CO.** The $^1$H−$^{15}$N HSQC spectrum of *pa*-HO−CO is shown in Figure 3, and the resonance assignments are listed in Table S1 of the Supporting Information. The majority of non-proline backbone amides were readily assigned following a strategy similar to that employed for assigning the backbone resonances of *pa*-HO−$N_3$ and *pa*-HO−CN.[25] A large majority of assignments were obtained using data sets acquired from triple resonance experiments carried out with a sample uniformly labeled with $^{15}$N and $^{13}$C, as has been outlined in the Experimental Methods section. The assignment of G125 was made with a sample of *pa*-HO−CO labeled selectively with $^{15}$N-Gly. Inspection of the $^1$H−$^{15}$N HSQC spectrum obtained from [$^{15}$N-Gly]-*pa*-HO−CO (Figure S1, Supporting Information), which shows cross-peaks originating exclusively from glycine residues, facilitated the identification of G125, as all other Gly residues in the sequence had been previously assigned with the aid of a suite of 3D heteronuclear experiments. It should be mentioned that the cross-peak identified as G125 in the HSQC spectrum of [$^{15}$N-Gly]-*pa*-HO−CO was observable in HSQC spectra obtained with protein labeled uniformly with $^{15}$N (inset in Figure 3). The cross-peak was initially overlooked, however, because of its weak intensity and unusual $^1$H chemical shift (~4.2 ppm). Nevertheless, the presence of the same cross-peak in HSQC spectra obtained from *pa*-HO−CO labeled selectively with $^{15}$N-Gly, together with inter-residue sequential correlations, made the assignment of this cross-peak unambiguous. Finally, it was not possible to obtain assignments for the N-terminal fragment comprising residues 1−12, likely because of line broadening brought about by intermediate exchange phenomena. In all, 177 out of 190 non-proline amide resonances were assigned.

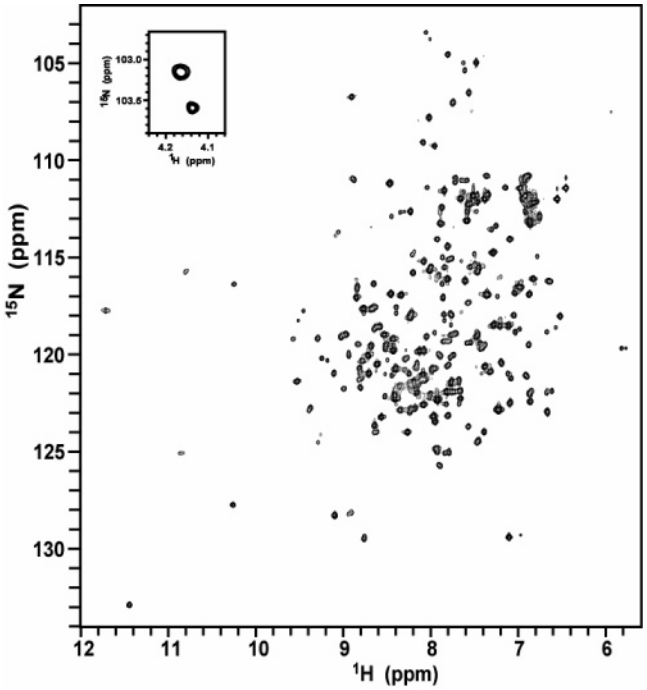


***Figure 3.*** $^1$H−$^{15}$N HSQC spectrum of 2.3 mM [U-$^{15}$N,$^{13}$C]-*pa*-HO−CO in 50 mM sodium phosphate, pH 7.0, and 5% $D_2O$. The inset shows the cross-peak originating from Gly125; the unusual chemical shifts are likely the influence of ring current effects from the heme macrocycle. The spectrum was obtained at 305 K using a Bruker Avance800 NMR spectrometer (see Experimental Methods). Complex points, 256 ($t_1$) × 2496 ($t_2$); spectral width, 2.6 kHz ($t_1$) × 19.2 kHz ($t_2$); 2 scans per increment; recycle delay, 1 s.

**Relaxation-Compensated Carr−Purcell−Meiboom−Gill Measurements.** A relatively recent and powerful approach to investigate conformational exchange occurring in the μs-to-ms time scale at the protein backbone level are the $^{15}$N rcCPMG (relaxation compensated Carr−Purcell−Meiboom−Gill)[60] and constant time relaxation compensated CPMG[53] experiments (CT-rc-CPMG). These experiments capitalize on the fact that conformational exchange on a μs-to-ms time scale results in modulation of the chemical shift of the $^{15}$N−H nucleus and is therefore a mechanism for transverse relaxation, $R_2$. In the absence of μs-to-ms conformational exchange the effective transverse relaxation rate, $R_2^{\text{eff}}(\nu_{\text{CPMG}})$, is independent of the CPMG pulse repetition rate $(\tau_{\text{CP}}\text{-}180°\text{-}\tau_{\text{CP}})_{n/2}$, where $\tau_{\text{cp}}$ is the spacing between 180° pulses, $n$ is an integer and $\nu_{\text{CPMG}} = 1/(4\tau_{\text{CP}})$.[59−61] In the presence of μs−ms conformational exchange, however, $R_2^{\text{eff}}(\nu_{\text{CPMG}})$ decreases with increasing $\nu_{\text{CPMG}}$. This stems from the fact that when the length of $\tau_{\text{CP}}$ is comparable to the lifetime of the conformations in chemical

(54) Farrow, N. A.; Zhang, O.; Forman-Kay, J. D.; Kay, L. E. *J. Biomol. NMR* **2004**, *4*, 727−734.
(55) Vialle-Printems, C.; van Heijenoort, C.; Guittet, E. *J. Magn. Reson.* **2000**, *142*, 276−279.
(56) Rodriguez, J. C.; Jennings, P. A.; Melacini, G. *J. Biomol. NMR* **2004**, *155*, 155−161.
(57) Das, R.; Abu-Abed, M.; Melacini, G. *J. Am. Chem. Soc.* **2006**, *128*, 8406−8407.
(58) Das, R.; Melacini, G. *J. Biol. Chem.* **2007**, *282*, 581−593.
(59) Mulder, F. A. A.; Skrynnikov, N. R.; Hon, B.; Dahlquist, F. W.; Kay, L. E. *J. Am. Chem. Soc.* **2001**, *123*, 967−975.
(60) Loria, J. P.; Rance, M.; Palmer, A. G. *J. Am. Chem. Soc.* **1999**, *121*, 2331−2332.
(61) Palmer, A. G. *Chem. Rev.* **2004**, *104*, 3623−3640.

exchange, asymmetric evolution of magnetization may occur about a given 180° pulse, which has the effect of interfering with echo formation. Consequently the measured relaxation rate, $R_2^{\text{eff}}$ ($\nu_{\text{CPMG}}$), includes its natural ($R_2^0$) and exchange ($R_{\text{ex}}$) contributions. On the other hand, when the length $\tau_{\text{CP}}$ is short relative to the lifetime of each of the conformations, the exchange process exerts no influence on individual echoes and the observed rate $R_2^{\text{eff}}$ ($\nu_{\text{CPMG}}$) approaches $R_2^0$.[62] Thus, the exchange contribution ($R_{\text{ex}}$) to the transverse relaxation is approximated by the difference $\Delta R^{\text{eff}}$ ($\nu_{\text{CPMG}}$), as indicated by eq 2.[60,62,63] As has been pointed out in the Experimental Methods section, per residue values of $\Delta R_2^{\text{eff}}$ ($\nu_{\text{CPMG}}$) were calculated using eq 1 from data obtained with $\nu_{\text{CPMG}}$ low = 25 Hz and $\nu_{\text{CPMG}}$ high = 600 Hz.

$$\Delta R_2^{\text{eff}}(\nu_{\text{CPMG}}) = [R_2(\nu_{\text{CPMG}}\ \text{low}) - R_2(\nu_{\text{CPMG}}\ \text{high})] \approx R_{\text{ex}} \qquad (2)$$

A per residue plot of the resultant $\Delta R_2^{\text{eff}}$ ($\nu_{\text{CPMG}}$) values is informative because amino acids exhibiting a positive $\Delta R_2^{\text{eff}}$ ($\nu_{\text{CPMG}}$) value are readily identified as undergoing conformational exchange in the $\mu$s−ms time scale, whereas residues not experiencing conformational motions in this time regime will display $\Delta R_2^{\text{eff}}$ ($\nu_{\text{CPMG}}$) values close to zero. Thus, $\Delta R_2^{\text{eff}}$ ($\nu_{\text{CPMG}}$) values obtained from measurements conducted with *pa*-HO−CN are shown in the per residue plot of Figure 4a. The horizontal full line is the average error obtained from two measurements, and the segmented horizontal lines represent 3 standard deviations above (or below) the mean. Clearly, several residues in *pa*-HO−CN exhibit $\Delta R_2^{\text{eff}}$ ($\nu_{\text{CPMG}}$) values that are higher than the threshold delimited by 3 standard deviations above the mean, which identifies them as undergoing conformational exchange (Figure 4a). The data indicate that sections of helices H3, H5, H6, H7, H9, H10, and H11, as well as the loop preceding helix 10, undergo conformational exchange in the $\mu$s−ms time scale. In comparison, similar experiments conducted with *pa*-HO−$N_3$ reveal that $\mu$s−ms conformational exchange in this complex is more restricted than in its *pa*-HO−CN counterpart (Figure 4b). Moreover, comparing the per residue plots in Figure 4a and b shows that most of the changes in conformational exchange between *pa*-HO−CN and *pa*-HO−$N_3$ take place in helices H3, H5, and H6; several residues harbored by these helices undergo conformational exchange in *pa*-HO−CN, whereas similar motions are suppressed in *pa*-HO−$N_3$.

Among residues located in the stretch of sequence 53−60 (H3) in *pa*-HO−CN, only residues Tyr53, Gln56, and Glu60 display cross-peaks that allow measurement of $R_2$'s. Cross-peak overlap or poor cross-peak intensity precludes reliable measurement of $R_2$'s for the remainder residues. It is thus not known whether residues 54−59 undergo conformational exchange. Figure 4a also shows that residues 79 (H5) and 81−83 (H6) do not appear to be dynamic, whereas the residues bracketing them (Arg78, Arg80, Ala84, and Arg85) undergo conformational exchange. Inspection of the structure (Figure 5) shows that all residues identified as undergoing conformational exchange in Figure 4a interact with one another, either by direct hydrogen bonds or mediated by hydrogen bonds to crystallographic water within the H-bonding network: The side chain of Gln56 is within hydrogen bond distance of water 29 (see Figure 5). Thus, if conformational changes of the Gln56 side chain modulate motions in its backbone, these movements can be propagated to the backbone of Glu60 (also undergoing conformational exchange) via a hydrogen bond between the Glu60 N−H and the carbonyl oxygen of Gln56. In a similar manner, the side chain of Arg80 interacts with water 52 (Figure 5). Conformational changes of the Arg80 side chain may modulate motions in its backbone, which are transmitted to the backbone of Arg84 via a hydrogen bond between its backbone N−H and the carbonyl oxygen of Arg 80. Another interesting path for propagation of motion among residues detected as undergoing conformational exchange can be traced starting with the carbonyl oxygen of Arg78, which is within hydrogen-bonding distance of water 29. The latter is within hydrogen-bonding distance of the Gln56 side chain (see above) and is also poised to interact with the hydroxyl group in the side chain of Ser 119 (see Figure 5). Thus, motions involving water 29, Gln56, and Arg78 can modulate motions in the side chain of Ser119, which can be propagated to its backbone and in turn to Ser122 via a hydrogen bond between the carbonyl oxygen of Ser119 and the N−H of Ser122. The details of how motions are coupled between water molecules, side chains, and backbone are not clear at present because the relaxation methods used in this study are sensitive only to backbone motions. Nevertheless, the fact that clear hydrogen bonding interactions connecting most of the residues undergoing conformational exchange can be traced strongly suggests that the motions detected by these experiments are linked via the network of hydrogen bonds in the structure of *pa*-HO.

It has been mentioned that analysis of protection factors obtained from H/D exchange experiments in the context of the structure and hydrogen-bonding network of *pa*-HO led to the suggestion that one function of this network is to allow conformational changes with minimum perturbation of the secondary structure.[25] In this context, the network of hydrogen bonds appears to play a significant structural role in HO, a role that imparts the enzyme with the necessary flexibility to adapt to the demanding changes in axial coordination and substrate structure modifications that take place during the catalytic cycle of heme degradation. Results from the relaxation studies reported herein, interpreted in the context of the hydrogen-bonding network of *pa*-HO, corroborate the notion that conformational and/or hydrogen bonding changes in the active site are propagated to key but remote structural elements in the enzyme via the hydrogen-bonding network. In addition, the relaxation studies suggest novel insights into the function of the network of structural waters in HO. Specifically, the results suggest that the nature of the axial ligand, by virtue of affecting the network of hydrogen bonds, exerts a significant level of control over the dynamic freedom experienced by the hydrogen-bonding network. To test this idea we prepared the Arg80Leu mutant of *pa*-HO (R80L-*pa*-HO), with the intention of disrupting key hydrogen bonding interactions and probing how these changes affect the dynamic behavior and reactivity of *pa*-HO. Findings from these investigations are presented in the following section.

**Disruption of the H-Bonding Network Causes nearly Global Chaotic Motions in *pa*-HO−$N_3$.** The R80L mutant of *pa*-HO was expressed to high yield in *E. coli*. The mutant

(62) Kempf, J. G.; Loria, J. P. In *Protein NMR Techniques*, 2nd ed.; Downing, A. K., Ed.; Humana Press: Totowa, NJ, 2004; Vol. 278, pp 185−231.
(63) Korzhnev, D. M.; Karlsson, B. G.; Orekhov, V. Y.; Billeter, M. *Protein Sci.* **2003**, *12*, 56−65.

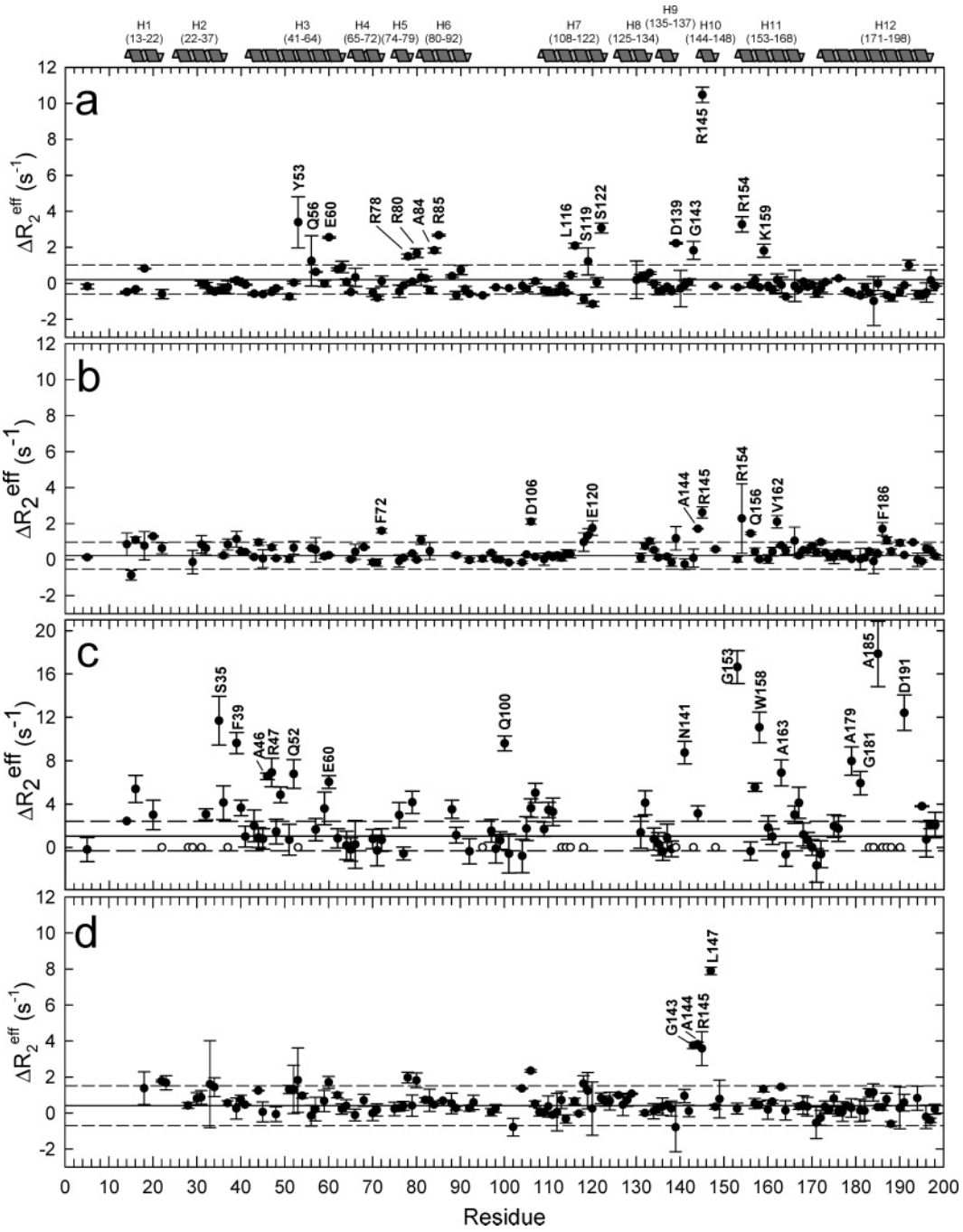


***Figure 4.*** Per residue effect of axial ligand coordination on the backbone $^{15}N$ relaxation dispersion $\Delta R_2^{eff}$ ($\nu_{CPMG}$) of *pa*-HO axially coordinated with (a) $CN^-$, (b) $N_3^-$, and (d) CO. The per residue plot in (c) shows values of $\Delta R_2^{eff}$ ($\nu_{CPMG}$) obtained for the R80L-*pa*-HO mutant coordinated with $N_3^-$, which was prepared with the aim of disrupting the hydrogen-bonding network in *pa*-HO. The horizontal line represents the average error obtained from two measurements, and the horizontal segmented lines represent 3 standard deviations above and below the average. Residues with $\Delta R_2^{eff}$ ($\nu_{CPMG}$) values more positive than the segmented line representing 3 standard deviations above the mean are considered to be in conformational exchange in the $\mu$s−ms time regime sampled by the ct-CPMG experiments utilized in these investigations.

enzyme exhibits UV−vis spectra characteristic of HO enzymes in its ferric, ferrous, and carbomonoxy ferrous states (Figure 6), which suggests that the environment near the heme has not been altered significantly. It is relevant, however, that, in contrast to the stability displayed by the oxyferrous complex of wild type *pa*-HO, the oxyferrous complex of the mutant is very susceptible to autoxidation (Figure S2). This susceptibility is presumably a consequence of having disrupted the hydrogen-bonding network, which prevents formation of key hydrogen bonds that stabilize the otherwise autoxidation-prone oxyferrous complex.

The efficiency of heme hydroxylation catalyzed by the R80L-*pa*-HO mutant relative to the wild type enzyme was probed by taking advantage of the surrogate reaction between resting state HO and $H_2O_2$. In this surrogate reaction ferric HO reacts with $H_2O_2$ to form the $Fe^{III}$−OOH intermediate, which hydroxylates the heme to meso-hydroxyheme (see Figure 2). In the presence of $O_2$ the latter is rapidly converted to verdoheme, whose

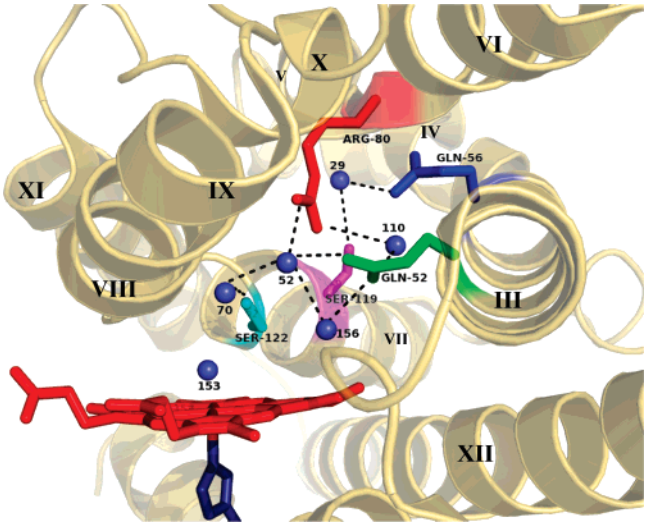


***Figure 5.*** View of *pa*-HO highlighting structural water molecules networked by hydrogen bonds to themselves and to side chains of key residues, some of which (Gln52, Gln56, and Arg80) are harbored by helices where $\mu$s−ms conformational exchange is observed in *pa*-HO−CN but not in *pa*-HO−$N_3$ or *pa*-HO−CO.

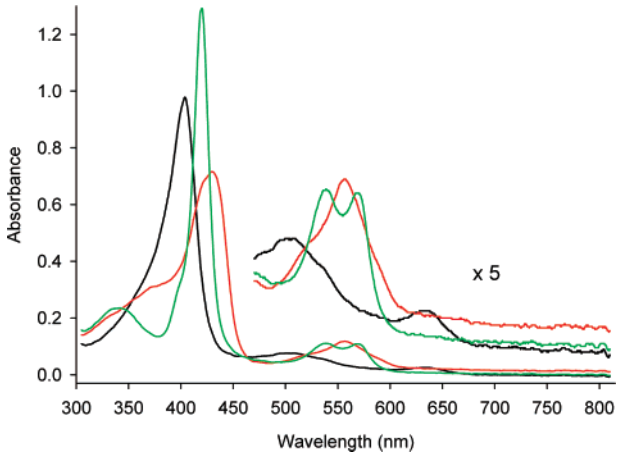


***Figure 6.*** Electronic absorption spectra of the R80L-*pa*-HO mutant in its resting, ferric (black), ferrous (red), and ferrous-CO state (green).

formation can be monitored by the appearance and growth of a band at 660 nm.[38,40,41] The time dependent formation of verdoheme upon addition of 1 equiv of $H_2O_2$ to wild type *pa*-HO is shown in Figure 7. In comparison, the R80L-*pa*-HO mutant uses $H_2O_2$ less efficiently because addition of 1 equiv of $H_2O_2$ results not only in slower formation of verdoheme but also in its significantly smaller accumulation (about half). These observations are in agreement with the important role attributed to the hydrogen-bonding network in controlling the reactivity of the $Fe^{III}$−OOH intermediate in HO enzymes.[34,35]

NMR investigations of the R80L mutant started with experiments aimed at assigning amide backbone resonances in the R80L-*pa*-HO−$N_3$ complex. These assignments (Table S2) were obtained by identifying sequential amide $H^N$ to $H^N$ NOEs in a $^1H-^{15}N$ NOESY-HSQC spectrum, using the assignments of the wild type protein[25] as a guide. Sequential NOE connectivities were observed for the vast majority of residues. Those not assigned occur in the segment comprising the site of mutation (i.e., residues 80 to 84), the N-terminal residues 1−12 (not assigned in WT), and those few residues for which assignments could not be obtained for the WT *pa*-HO−$N_3$ complex.[25] Clear

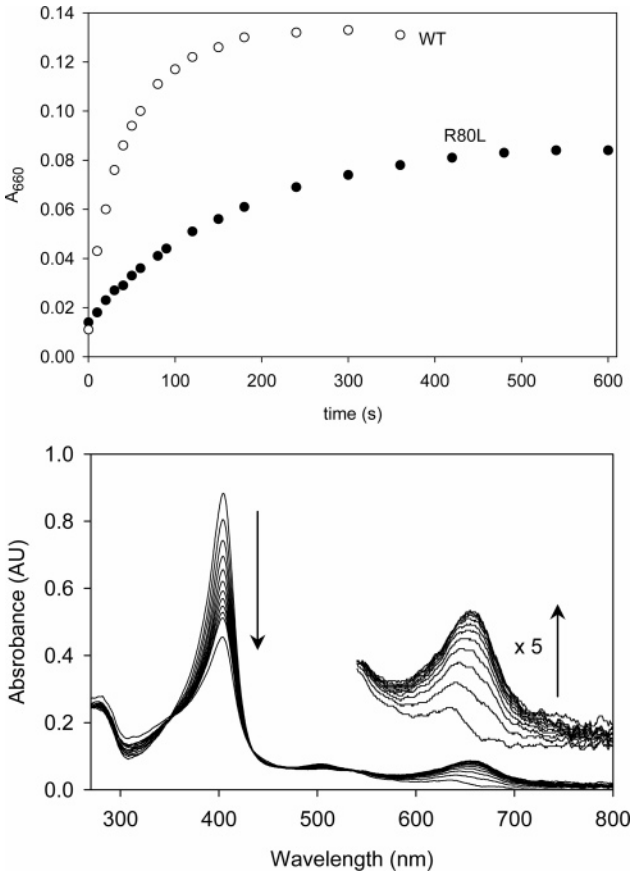


***Figure 7.*** Top: (○) Time dependent oxidation of the heme in wild type *pa*-HO to verdoheme upon addition of 1 equiv of $H_2O_2$, as monitored by appearance and increase in absorbance of the band at 660 nm, which is diagnostic for verdoheme. (●) Time dependent oxidation of the heme in the R80L-*pa*-HO mutant to verdoheme upon addition of 1 equiv of $H_2O_2$. Bottom: Changes in the electronic absorption spectrum of the R80L mutant upon addition of 1 equiv of $H_2O_2$.

manifestations of conformational exchange affecting the R80L-*pa*-HO−$N_3$ mutant are evident in a number of cross-peaks in its $^1H-^{15}N$ HSQC spectrum (Figure S3), which exhibit weaker intensities relative to their counterparts in the HSQC spectrum of wild type *pa*-HO−$N_3$. Examples of these peaks can be readily seen in the downfield shifted resonances corresponding to backbone N−H of R145 and H146. Although these groups are located sufficiently removed from the heme, so as to be unaffected by the paramagnetism of the heme iron, their corresponding cross-peaks exhibit significant temperature dependence (Figure 8). In addition, these cross-peaks are most intense at the lowest temperature explored (8 °C) and become progressively less intense, or disappear, as the temperature is increased (see Figure S4). This behavior suggests chemical exchange in a time regime approaching the coalescence point. Thus, at the lower temperatures H146 is in slow exchange, near the coalescence point; only one cross-peak is observed due to the large asymmetry in the population of the interconverting conformers. As the temperature increases, the spin system reaches the coalescence point and the cross-peak becomes undetectable. Similar observations are made with the backbone N−H cross-peak of R145, except that at the maximum accessible temperature these spin systems have not yet reached the coalescence point (Figure S4). In comparison, the effects of temperature changes on the chemical shifts and intensities of equivalent cross-peaks in the spectrum of wild type pa-HO−

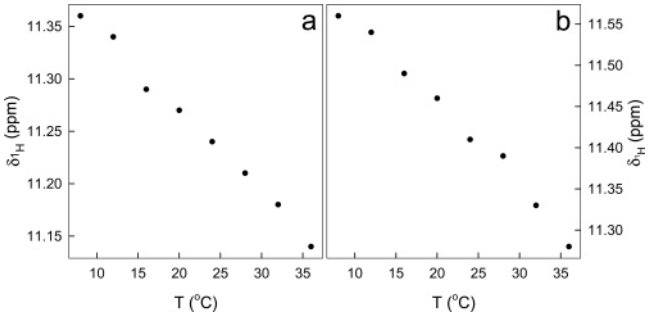


***Figure 8.*** Temperature dependence of the amide $^1$H chemical shift from R145 (a) and H146 (b) in the R80L-*pa*-HO−$N_3$ complex. The corresponding changes in cross-peak intensity and chemical shifts are presented in Figure S3.

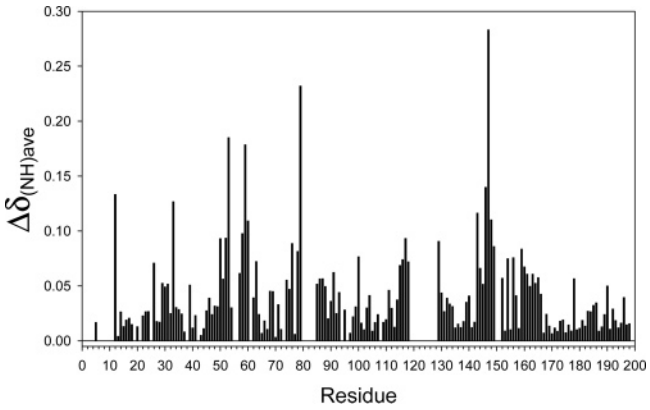


***Figure 9.*** Per residue chemical shift difference expressed as $\Delta\delta$, obtained by subtracting the chemical shift of a residue in the *pa*-HO−$N_3$ complex from the corresponding chemical shift in the R80L-*pa*-HO−$N_3$ mutant. The differences in amide chemical shifts are the weighed average of $^1$H and $^{15}$N shifts, calculated with the expression: $\Delta\delta_{av} = \{[(\Delta\delta_{^1H})^2 + (\Delta\delta_{^{15}N}/5)^2]/2\}^{1/2}$.

$N_3$ are nearly negligible (Figure S4). The R80L mutation also induces the readily distinguishable dynamic behavior manifested in the side chain of W158. $N_z$ exchange experiments reveal cross-peaks involving a major conformer of the indole N−H group and a minor population only discernible from the presence of the exchange cross-peak (Figure S5); similar cross-peaks are absent in $N_z$ exchange spectra from wild type *pa*-HO−$N_3$. As will be shown below, the distinct dynamic behavior of the W158 side chain between the R80L mutant and the WT protein is likely a manifestation of enhanced backbone $\mu$s−ms conformational exchange in helix XI induced by the mutation.

The enhanced relaxation characteristics exhibited by many cross-peaks in the HSQC spectrum of R80L-*pa*-HO−$N_3$ are consistent with the large number of residues undergoing $\mu$s−ms conformational exchange, as indicated by their positive $\Delta R_2^{\text{eff}}(\nu_{\text{CPMG}})$ values in the per residue plot of Figure 4c. In fact, comparing the data in plot Figure 4c with that obtained for wild type *pa*-HO−$N_3$ (4b) leads to the unavoidable conclusion that disruption of the hydrogen-bonding network in *pa*-HO promotes $\mu$s−ms conformational motions in virtually the entire structure. In this context, it is important to note that the CT-rc-CPMG experiments conducted with R80L-*pa*-HO−$N_3$ were performed under similar conditions of protein concentration (∼1.7 mM) and temperature (32 °C) as those with wild type *pa*-HO−$N_3$. Nevertheless, a relatively large number of residues in the mutant could not be included in the analysis of relaxation data because the corresponding cross-peaks exhibit poor signal-to-noise ratios due to enhanced relaxation rates, which preclude reliable measurements of their intensities. For comparative purposes, these residues and those for which assignments could not be made in the R80L mutant, but are amenable to relaxation studies in the wild type protein, are represented with open circles in the per residue plot of Figure 4c.

Chemical shift perturbation analysis of the mutant was carried out with the intention of uncovering potential changes in structure caused by replacing R80 for L. This was performed by calculating weighted averages of the differences in amide chemical shifts ($\Delta\delta_{\text{NH, ave}}$) between R80L-*pa*-HO−$N_3$ and wild type *pa*-HO−$N_3$ (Figure 9). This analysis shows only marginal effects on the structure, with the most significant perturbations affecting residues 53, 59, 74, 79, 143, and 147, which are located in the general volume surrounding the mutation. It is thus striking that the effects of replacing R80 for L on $\mu$s−ms dynamics have little or no correlation with the structural perturbations suggested by the $\Delta\delta$ values. Instead, many residues far removed from the immediate vicinity of residue 80 exhibit dramatically enhanced $\mu$s−ms dynamics in the mutant relative to the wild type protein. Hence, the remarkable nearly global induction of $\mu$s−ms conformational fluctuations caused by the Arg80 to Leu mutation provides compelling evidence implicating the side chain of R80 and, by extension, the hydrogen-bonding network, as an essential structural motif that functions, among other things, to modulate the equilibrium conformational dynamics of heme oxygenase.

**The distal helix in *pa*-HO−CO is rigid in the $\mu$s−ms time scale.** Results from performing CT-rc-CPMG studies with a sample of *pa*-HO−CO are shown in Figure 4d. The data summarized in this per residue plot indicates that conformational exchange in *pa*-HO−CO is limited mostly to helix H10. This suggests that the residues involved in the network of hydrogen bonds, which undergo conformational exchange in *pa*-HO−CN and not in *pa*-HO−$N_3$, are also devoid of $\mu$s−ms motions in *pa*-HO−CO. This observation is in agreement with the notion that changes in the hydrogen-bonding status brought about by the different geometrical and hydrogen-bonding preferences of distal ligands coordinated to the heme iron exert influence in the dynamical properties of residues along the path of the network, which starts at the active site and extends to the surface of the enzyme (see Figure 5).

The diamagnetic nature of the *pa*-HO−CO complex makes it possible to assign resonances from residues immediately above the heme iron, a task that is significantly more difficult or even impossible in the paramagnetic ferric enzymes. In the particular case of *pa*-HO−CN and *pa*-HO−$N_3$, significant effort was placed in the assignment of residues located on the helix kink above the heme iron, i.e., residues 123−127. Despite this effort, assignments were obtained for only a few of these residues, and in the case of Gly125, only the $^{15}$N resonance was assigned on the basis of 1-D $^{15}$N experiments carried out with $^{15}$N-Gly labeled samples.[25] Consequently, the dynamic behavior of these residues cannot be studied with the relaxation experiments used in this work. In contrast, these residues have been assigned in the *pa*-HO−CO complex and the corresponding cross-peaks have been utilized to assess conformational exchange in the $\mu$s−ms regime, as sampled by CT-rc-CPMG experiments. Inspection of the per residue plot in Figure 4d indicates that residues 123−127 (helix kink), as well as residues in the two helices that flank it (H7 and H8), do not undergo conformational exchange.

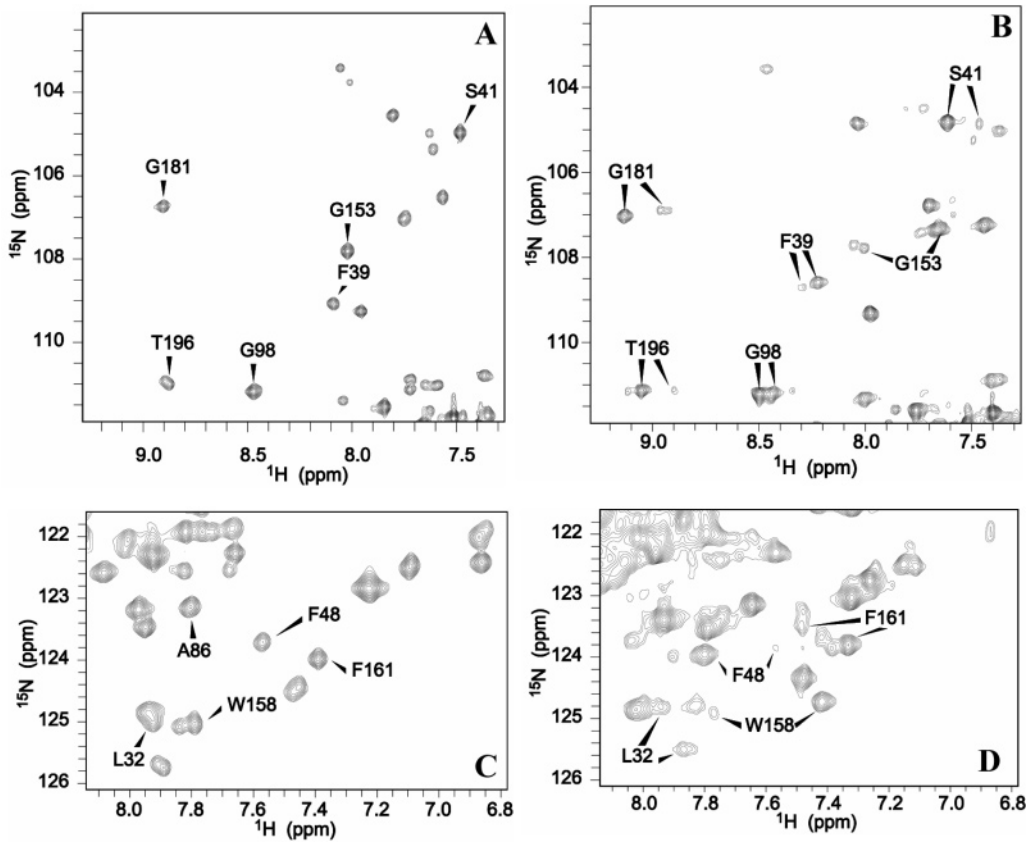


***Figure 10.*** (A and C) Representative expansions of the $^{1}$H−$^{15}$N HSQC spectrum of [U-$^{15}$N]-*pa*-HO−CO. (B and D) Equivalent expansions from the $^{1}$H−$^{15}$N HSQC spectrum of [U-$^{15}$N]-R80L-*pa*-HO−CO highlighting several residues exhibiting "double" cross-peaks. The side-by-side comparisons of (A) and (B) and then (C) and (D) reveal conformational disorder in the R80L-*pa*-HO−CO mutant that is absent in wild type *pa*-HO−CO.

CPMG-based experiments of the type used in the current studies serve to identify N−H groups whose $^{15}$N shift is modulated by chemical exchange processes taking place at a microsecond to millisecond time scale. Collectively, phenomena not necessarily associated with a change in the position of the N−H vector in relation to a reference frame could in principle induce chemical shift modulation. For instance, the presence of variable ring currents and electrostatic fields near an NH amide group has been known to affect the chemical shift of amide nitrogens.[64] Consequently, potential contributions from such factors must be considered when interpreting relaxation data derived from CPMG experiments.[64] Regions near the heme in *pa*-HO are likely affected by ring currents stemming from the heme, as suggested by the high-field biased amide proton shifts of G125 (4.2 ppm) and A126 (6 ppm). Nevertheless, the $^{15}$N relaxation behavior of the segment spanning residues 123 to 126 was found to be virtually insensitive to $\nu_{CPMG}$ field strength, indicating that, while present, ring current effects do not lead to $^{15}$N chemical shift modulation of the involved amide groups at the $\mu$s−ms time scale. Thus, the stillness of this helix in this time scale is relevant in the context of the mechanism of heme oxygenation by HO, as the ferrous CO complex of HO is thought to emulate the oxyferrous form of the enzyme. In this regard, the $\nu_{CPMG}$ field independence exhibited by the $^{15}$N relaxation of the NH groups of residues 120−126 in *pa*-HO−CO can be taken to denote rigidity in the $\mu$s−ms time scale. This finding is consistent with the notion that these residues help in stabilizing the hydrogen bond network in the oxyferrous ($Fe^{II}-O_2$) complex prior to reduction by a second electron and subsequent electron rearrangement that converts the coordinated $O_2$ ligand into the ferric peroxo ($Fe^{III}-OO^-$) intermediate. These findings and the relatively rapid autoxidation of the oxyferrous complex of R80L-*pa*-HO (see above) suggest that disruption of the hydrogen-bonding network should also be manifested in conformational disorder in the R80L-*pa*-HO−CO complex. Results from investigations aimed at probing this idea are described in the following section.

**Disruption of the H-bonding network causes conformational disorder in *pa*-HO−CO.** The $^{1}$H−$^{15}$N HSQC spectrum of R80L-*pa*-HO−CO is shown in Figure S6 (sequential assignments are summarized in Table S3), where it is compared with the HSQC spectrum of wild type *pa*-HO−CO. A number of cross-peaks in the spectrum of the R80L-pa-HO−CO complex are absent or exhibit weaker relative intensities compared to their counterparts in the HSQC spectrum of wild type *pa*-HO−CO. Even more striking is the fact that several cross-peaks in the spectrum of R80L-pa-HO−CO are doubled, which suggests significant population of at least two conformations in several segments of the structure. The presence of double peaks is illustrated in expanded portions of the HSQC spectrum obtained from R80L-*pa*-HO−CO (Figure 10B and 10D), which are presented adjacent to equivalent expansions of the HSQC spectrum of wild type pa-HO−CO (Figure 10A and C), in order to demonstrate that only the mutant is conformationally disordered. Evidence demonstrating that the doubling of peaks originates from conformational disorder in the R80L-*pa*-HO−

(64) Wang, L.; Pang, Y.; Holder, T.; Brender, J. R.; Kurochkin, A. V.; Zuiderweg, E. R. P. *Proc. Natl. Acad. Sci. U.S.A.* **2001**, *98*, 7684−7689.

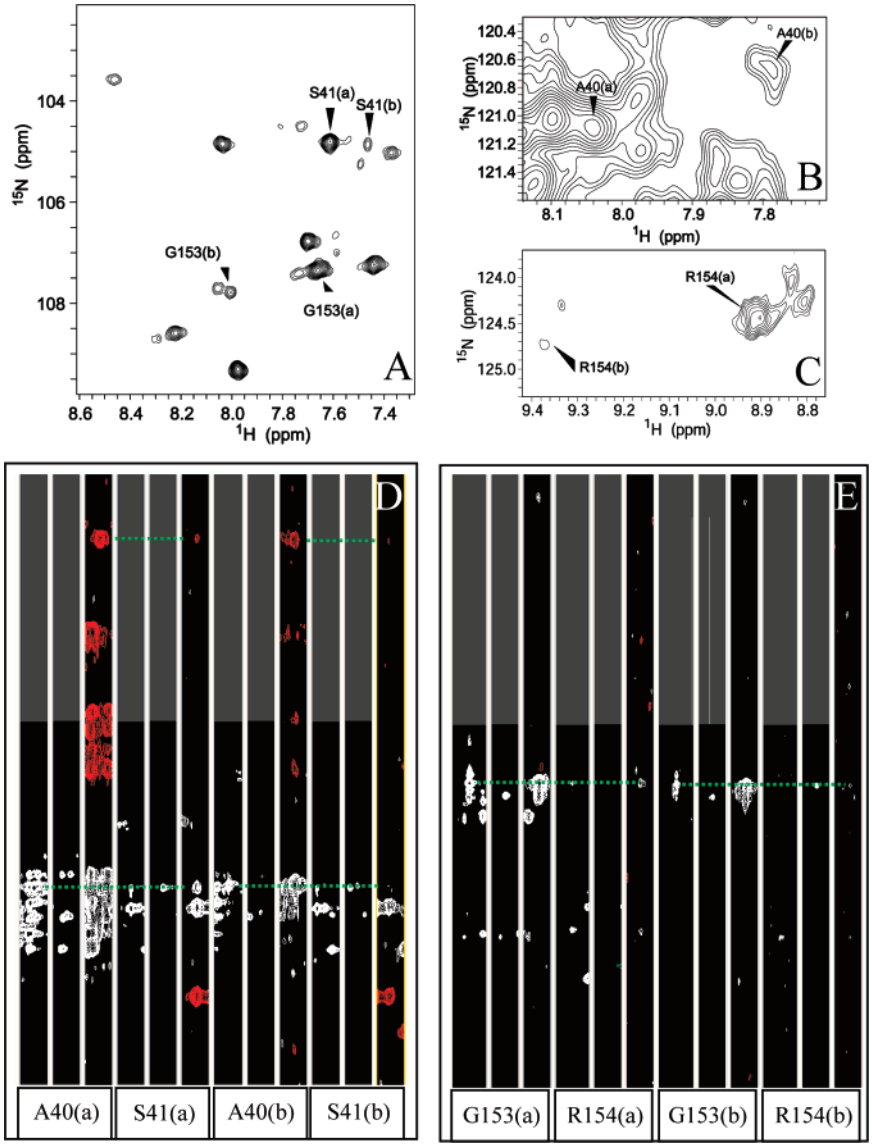


***Figure 11.*** (A−C) Representative expansions of the $^{1}$H−$^{15}$N-HSQC spectrum obtained with a sample of [U-$^{15}$N]-R80L-*pa*-HO−CO. Cross-peaks labeled S41(a), S41(b), etc., originate from the same residue in different conformations. (D) Strip plots taken from $^{1}$H−$^{13}$C slices of triple resonance spectra used to perform the sequential resonance assignments of the R80L-*pa*-HO−CO complex. The first three strips were taken at the $^{15}$N frequency corresponding to the N−H cross-peak of A40(a) and are presented in the order HNCA, HN(CO)CA, and HNCACB. The subsequent three strip plots are presented in the same order but were taken at the $^{15}$N frequency corresponding to the N−H cross-peak of S41(a). The green dotted lines, included to guide the eye, indicate correlations between A40(a) and S41(a). Correlations between A40(b) and S41(b) can be obtained in a similar manner, starting with the seventh strip plot. (E) Strip plots correlating G153(a) with R154(a) and G153(b) with R154(b).

CO complex is presented next: Panel A in Figure 11 highlights two sets of "double" cross-peaks for Ser41 and Gly153; each set is labeled (a) and (b) to emphasize the fact that the cross-peaks originate from different conformations of the same residue. Panels B and C show two sets of cross-peaks corresponding to Ala40(a), Ala40(b), Arg154(a), and Arg154(b). Each of the cross-peaks in the set corresponding to Ala40 can be correlated to a cross-peak in the set corresponding to Ser41 by the strip plots taken from $^{1}$H−$^{13}$C slices in the HNCA, HN(CO)CA, and HNCACB spectra used to make sequential assignments. For instance, the strip plot corresponding to the $^{15}$N frequency of Ala40(a) in the HNCA spectrum (the first strip in panel D) is followed by strip plots from HN(CO)CA and HNCACB spectra taken at the same $^{15}$N frequency (second and third strips). These are followed by strip plots taken at the $^{15}$N frequency of Ser41(a) from HNCA, HN(CO)CA, and HNCACB spectra (strips fourth to sixth). The remainder strip plots in panel D (seventh to twelfth) were organized in a similar fashion but start with the strip plot taken from the HNCA spectrum at the $^{15}$N frequency of Ala40(b). HNCA and HNCACB spectra provide intra- and inter-residue correlations between the amide NH and the $^{13}C_{\alpha}$ and/or $^{13}C_{\beta}$ nuclei of the same and preceding residue, respectively. HN(CO)CA spectra, on the other hand, show exclusively inter-residue correlations between the amide NH and the $^{13}C_{\alpha}$ of the preceding residue. Consequently, the cross-peak in the HN(CO)CA strip of S41(a) (fifth strip in panel D) correlates S41(a) with A40(a), as shown by the green dotted line included to guide the eye. In a similar manner, the cross-peak in the HN(CO)CA strip of S41(b) (eleventh strip in panel D) correlates S41(b) with A40(b). Cross-peaks in red have a sign opposite that of cross-peaks in white and represent correlations between the amide NH and $^{13}C_{\beta}$ nuclei of the same and preceding residue in HNCACB spectra. Hence, cross-peaks at the same $^{1}$H−$^{13}$C coordinates in the strips corresponding to

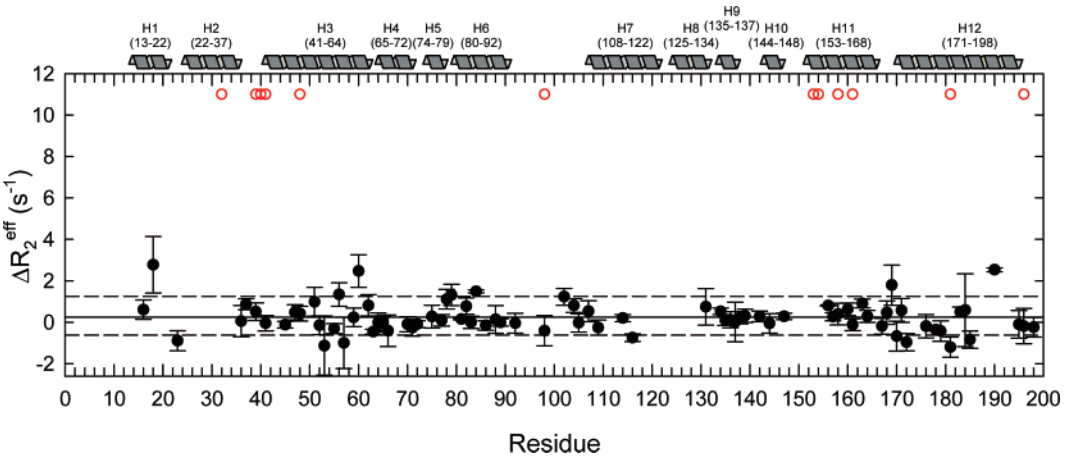


***Figure 12.*** Per residue plot of $\Delta R_2^{\text{eff}}$ ($\nu_{\text{CPMG}}$) obtained from the R80L-*pa*-HO−CO complex (see caption to Figure 4 for details). The red circles represent residues exhibiting "double" cross-peaks in the HSQC spectrum of the complex.

the HNCACB spectrum taken at $^{15}$N frequencies corresponding to A40(a) and S41(a) (third and sixth strips) and frequencies corresponding to A40(b) and S41(b) (ninth and twelfth strips) corroborate the correlations. Similar observations correlating G153(a) with R154(a) and G153(b) with G154(b) are shown in panel E.

Given the conformational disorder implicit in the HSQC spectrum of the R80L-*pa*-HO−CO complex, it was surprising that the CT-rc-CPMG studies conducted with this molecule showed that most residues do not exhibit positive $\Delta R_2^{\text{eff}}$ ($\nu_{\text{CPMG}}$) values (Figure 12). This observation, which is in stark contrast to observations made with the R80L-pa-HO−$N_3$ complex (see Figure 4c), indicates that conformational interconversion in the R80L-*pa*-HO−CO complex does not occur in the $\mu$s−ms regime accessible to the CT-rc-CPMG experiments. It is important to note that the red circles in Figure 12 represent residues with well-resolved "double" cross-peaks in the HSQC spectrum of the R80L-*pa*-HO−CO complex. This information was included in Figure 12 to show that the conformational disorder implicit in these features of the spectrum affect several sections of the *pa*-HO fold. In this context, it is also important to mention that the number of "double" cross-peaks is larger than that shown in Figure 12 because peaks located in crowded regions of the spectrum were omitted from the analysis. It is therefore possible to ascertain that disruption of the hydrogen-bonding network causes conformational disorder in *pa*-HO. The time scale of the resultant conformational dynamics, however, depends on the oxidation state of the heme-iron and on the nature of the distal ligand. In an attempt to approximate the time scale of conformational exchange in the R80L-*pa*-HO−CO complex, several $N_z$ exchange spectra were acquired with mixing times ranging from 1 to 300 ms (data not shown). The absence of exchange cross-peaks correlating signals originating from conformations (a) and (b) indicate that the residence time of each of the (a) and (b) conformers is larger than 300 ms.

## Discussion

A recent study reported the sequential backbone NMR assignments of the ferric cyanide- and azide-inhibited forms of *pa*-HO, which allowed global probing of the polypeptide by means of H/D exchange experiments.[25] A comparative analysis of protection factors obtained from H/D exchange rate constants showed that *pa*-HO−$N_3$ exhibits significantly higher protection to exchange than *pa*-HO−CN. Interestingly, the higher protection factors in *pa*-HO−$N_3$ were not confined to the immediate vicinity of the heme pocket; rather, it was found that many residues exhibiting higher protection factors are located near the protein surface, far removed from the heme and the distal ligand. These observations were interpreted to suggest that changes brought about near the heme upon substitution of $CN^-$ for $N_3^-$ in the distal pocket of *pa*-HO trigger an attenuation of flexibility via propagation of minor structural rearrangements along the network of hydrogen-bonded waters characteristic of HO.[25] In the study reported herein we applied relatively recently developed NMR methodology[53,60] aimed at extracting the presence of $\mu$s−ms conformational exchange in proteins and enzymes to probe the idea that *pa*-HO undergoes dynamical changes in response to the nature of the axial ligand.

Three distinct axial coordination states were studied in an attempt to gain insight regarding potential changes in polypeptide conformational freedom along the catalytic cycle of dioxygen activation that leads to heme degradation (see Figure 2). Thus, *pa*-HO−CN was studied as an approximation of the resting state of the enzyme, the *pa*-HO−CO complex, as a mimic of the oxyferrous complex, and the *pa*-HO−$N_3$ complex, in lieu of the extremely reactive $Fe^{III}$−OOH complex. The *pa*-HO−CN complex exhibits the largest conformational freedom in the $\mu$s−ms time scale. Replacing the $CN^-$ ligand for $N_3^-$ lowers the conformational freedom of the polypeptide, as can be seen from comparing Figure 4a and b. As pointed out, the changes in conformational dynamics affect residues involved in stabilizing key water molecules in the hydrogen-bonding network. In this context, studies conducted with the *pa*-HO−$N_3$ complex to gain insight regarding the elusive $Fe^{III}$−OOH intermediate revealed that coordination of $N_3^-$ to *pa*-HO results in unusual heme electronic structures that are expected to prime heme reactivity.[33,43] The unusual heme electronic structures are likely triggered by formation of a hydrogen bond between the amide hydrogen of Gly125 and the coordinating nitrogen of the $N_3^-$ ligand.[25] Hence, the coordination state and associated electronic structure (reactivity) of the active site are propagated via the hydrogen-bonding network and ultimately affect the conformational freedom of key but remote elements in this network. It is thus tempting to speculate that if the electronic

structure and dynamic behavior of the $Fe^{III}-OOH$ intermediate are similar to those of *pa*-HO$-N_3$, the relative "conformational rigidity" of key elements in the hydrogen-bonding network allows the enzyme to protonate the nascent $Fe^{III}-OO^-$ to form the heme hydroxylating species, $Fe^{III}-OOH$, and avoid formation of $Fe^{III}-OOH_2$, which would be expected to rapidly decay into a ferryl species. The latter is involved in peroxidase and monooxygenase chemistry but does not participate in the catalytic cycle of heme degradation.[65]

The notion that the polypeptide changes its conformational freedom in response to the type of axial ligand coordinating the heme iron is also supported by changes in the $\mu$s$-$ms conformational freedom observed upon replacing the ferric$-$CN species with the ferrous$-$CO complex. In this case, comparing Figure 4a and d also shows that $\mu$s$-$ms conformational motions in helices H3, H5, and H6 of the *pa*-HO$-$CN complex become attenuated in *pa*-HO$-$CO, which was studied as a surrogate of the oxyferrous complex. These findings are relevant to the current understanding of the catalytic cycle because they imply that stabilization of the $O_2$ ligand requires a relatively organized (more rigid) network of hydrogen bonds. In fact, the oxyferrous complex of R80L-*pa*-HO is autoxidized completely in less than 2 min, whereas the oxyferrous complex of wild type *pa*-HO is significantly more stable. Hence, the findings reported herein show that the hydrogen-bonding network in HO is a highly malleable structural element that functions by permitting HO to rapidly adapt to the changes in the distal coordination state imposed by the complicated nature of the catalytic cycle. Adaptation is likely facilitated by rearrangement of hydrogen bonding interactions and perhaps key side chain conformations. These types of rearrangements have been seen in "static" X-ray crystal structures of mammalian and bacterial HOs, when comparing structures in the ferric state, distally coordinated by $H_2O$,[23,28,29,66] $CN^-$,[49] or $N_3^-$,[24] and the ferrous state, either five-coordinate[29,49,66] or coordinated by CO,[36,49] $O_2$,[49] or NO.[36,66] The results reported herein indicate that these rearrangements likely take place in the $\mu$s$-$ms time scale, which is the time regime that would be expected if these motions are involved in aiding the catalytic cycle.

The observed changes in conformational flexibility, interpreted in the context of rearrangements of the hydrogen-bonding network, also suggest that the latter functions to modulate conformational freedom in sections of the polypeptide that participate in the network. This idea was tested by studying the effects of disrupting the hydrogen bond network on polypeptide dynamics. The results from these investigations are striking because the mutant (R80L-*pa*-HO$-N_3$) exhibits nearly global $\mu$s$-$ms conformational disorder (Figure 4c), which is not existent in the wild type *pa*-HO$-N_3$ complex (Figure 4b). In comparison, the R80L-*pa*-HO$-$CO complex experiences significant conformational disorder in a time scale much slower than that characteristic of the motions in the R80L-*pa*-HO$-N_3$ complex. The striking difference in the time scale of conformational dynamics between the $N_3^-$ and CO complexes of the R80L mutant of *pa*-HO strongly suggests that the heme-iron oxidation state, as well as the nature of the distal ligand, exerts control on the conformational flexibility of the enzyme. The findings, therefore, indicate that an important function of the network of hydrogen bonds in HO is to restrain the global conformational freedom of the enzyme and to tune the conformational mobility needed to accomplish each of the distinct chemical transformations demanded by the catalytic cycle. It is therefore interesting to consider that the fold of HO evolved to be highly dynamic, which in the case of the apoprotein facilitates the binding of a very large substrate (heme). Hence, when the enzyme is not engaged in catalysis (resting state), there is a significant amount of conformational disorder. However, as the enzyme starts along the path of the catalytic cycle, the different axial ligands that bind to the heme iron promote the necessary conformational order and dynamic restraint (tuning) that allows the efficient chemical transformations needed to break the heme macrocycle. The information needed to tune the dynamic freedom of the polypeptide is communicated from the active site to the polypeptide via the hydrogen-bonding network. The suggestion made here that the enzyme in its resting state ($H_2O$ at the distal site) is significantly more conformationally active than the cyanide-inhibited form studied here finds support in preliminary observations from investigations aimed at probing the dynamical properties of the polypeptide in the resting state ($S = {}^5/_2$). These results, once in final form, will be communicated elsewhere.

**Acknowledgment.** This work was supported by grants from the National Science Foundation (MCB-0446326) and the National Institutes of Health (GM-50503 and RR-017708). The authors thank Dr. Giuseppe Melacini, McMaster University, for insightful discussions.

**Supporting Information Available:** NMR data including an HSQC spectrum of [$^{15}$N-Gly]-*pa*-HO$-$CO, [U-$^{15}$N,$^{13}$C]-R80L-*pa*-HO$-N_3$, differences in autoxidation rate between the oxyferrous complex of wild type- and R80L-*pa*-HO, portions of HSQC spectra obtained with this mutant at different temperatures, portions of $N_z$ exchange spectra of ferric wild type [U-$^{15}$N]-*pa*-HO$-N_3$ and [U-$^{15}$N]-R80L-*pa*-HO$-N_3$, side-by-side comparisons of HSQC spectra obtained with the CO complex of wild type and R80L *pa*-HO, and tables listing the backbone ($^{15}N^H$, $^1H^N$, $C_\alpha$ and $C_\beta$) resonance assignments of *pa*-HO$-$CO, amide ($^{15}N^H$ and $^1H^N$) resonance assignments of R80L-*pa*-HO$-N_3$, and backbone resonance assignments of R80L-*pa*-HO$-$CO. This material is available free of charge via the Internet at http://pubs.acs.org.

JA072405Q

(65) Matsui, T.; Kim, S. H.; Jin, H.; Hoffman, B. M.; Ikeda-Saito, M. *J. Am. Chem. Soc.* **2006**, *128*, 1090−1091.
(66) Lad, L.; Wang, J.; Li, H.; Friedman, J.; Bhaskar, B.; Ortiz de Montellano, P. R.; Poulos, T. L. *J. Mol. Biol.* **2003**, *330*, 527−538.